Biogeosciences Discuss., 9, 13243–13286, 2012
www.biogeosciences-discuss.net/9/13243/2012/
doi:10.5194/bgd-9-13243-2012

Biogeosciences Discussions

Impact of an 8.2-kyr-like event on methane emissions in northern peatlands

S. Zürcher[1,2], **R. Spahni**[1,2], **F. Joos**[1,2], **M. Steinacher**[1,2], **and H. Fischer**[1,2]

[1]Climate and Environmental Physics, Physics Institute, University of Bern, Sidlerstrasse 5, 3012 Bern, Switzerland
[2]Oeschger Centre for Climate Change Research, University of Bern, Zähringerstrasse 25, 3012 Bern, Switzerland

Received: 18 July 2012 – Accepted: 12 September 2012 – Published: 25 September 2012

Correspondence to: S. Zürcher (zuercher@climate.unibe.ch)

Published by Copernicus Publications on behalf of the European Geosciences Union.

Abstract

Rapid changes in atmospheric methane (CH_4), temperature and precipitation are documented by Greenland ice core data both for glacial times (the so called Dangaard-Oeschger (DO) events) as well as for a cooling event in the early Holocene (the 8.2 kyr event). The onsets of DO warm events are paralleled by abrupt increases in CH_4 by up to 250 ppbv in a few decades. Vice versa, the 8.2 kyr event is accompanied by an intermittent decrease in CH_4 of about 80 ppbv over 150 yr. The abrupt CH_4 changes are thought to mainly originate from source emission variations in tropical and boreal wet ecosystems, but complex process oriented bottom-up model estimates of the changes in these ecosystems during rapid climate changes are still missing. Here we present simulations of CH_4 emissions from northern peatlands with the LPJ-Bern dynamic global vegetation model. The model represents CH_4 production and oxidation in soils and transport by ebullition, through plant aerenchyma, and by diffusion. Parameters are tuned to represent site emission data as well as inversion-based estimates of northern wetland emissions. The model is forced with climate input data from freshwater hosing experiments using the NCAR CSM1.4 climate model to simulate an abrupt cooling similar to the widespread 8.2 kyr event. As a main result we get a concentration reduction of ~ 10 ppbv per degree K change of mean northern hemispheric surface temperature in peatlands. This sensitivity comprises effects on peatland emissions of similar size by the temperature itself as well as by the accompanying change in precipitation rate, hence water table. Comparison with the ice core record reveals that a change in boreal peatland emissions alone could not completely account for the 80 ppbv methane decline during the 8.2 kyr event, pointing to a significant contribution from tropical wetlands to this event.

BGD

9, 13243–13286, 2012

1 Introduction

CH_4 is a greenhouse gas contributing to the ongoing global warming. CH_4 concentrations have increased from their preindustrial value of ∼ 700 ppbv to approximately 1800 ppbv in 2008 (Dlugokencky et al., 2009) due to anthropogenic CH_4 emissions. Air enclosures in polar ice cores allows for the reconstruction of methane variations in the past and show that CH_4 changed in concert with Northern Hemisphere temperature during the glacial/interglacial transitions (Loulergue et al., 2008) as well as during rapid climate variations. Examples of abrupt CH_4 variations recorded in Greenland ice cores are the 8.2 kyr event in the early Holocene (Fig. 1) (Blunier et al., 1995; Chappellaz et al., 1997; Spahni et al., 2003; Kobashi et al., 2007), the Dansgaard-Oeschger events (D-O-events) in the glacial period (Chappellaz et al., 1993; Brook et al., 2000; Blunier and Brook, 2001; Flückiger et al., 2004; Huber et al., 2006; Baumgartner et al., 2012) or the Younger Dryas (YD) cooling event (Chappellaz et al., 1993; Baumgartner et al., 2012). During the last glacial period Greenland temperature and CH_4 are found to covary within ∼ 30 yr, which is the limit of ice core data resolution and the width of the age distribution of air enclosed in bubbles in the ice (Huber et al., 2006). This suggests that CH_4 sources responded synchronously to the rapid climate changes. The nominal sensitivity of methane concentration variations on changes in Greenland temperature derived from ice cores is about ∼ 22 ppbv K^{-1} for the 8.2 kyr event (Kobashi et al., 2007), ∼ 7–16 ppbv K^{-1} for onsets of D-O events (Huber et al., 2006) and ∼ 9 ppbv K^{-1} for the beginning and end of the YD (Severinghaus et al., 1998; Brook et al., 2000; Grachev and Severinghaus, 2005). Note, however, that temperature changes recorded in Greenland are not necessarily representative for the temperature changes in boreal and even less in tropical wetland sources nor for precipitation changes.

While the origin of the abrupt climate variations can be explained by a shut-down or resumption of the North Atlantic thermohaline circulation (Vellinga and Wood, 2002; McManus et al., 2004; Ellison et al., 2006), the origin of atmospheric methane variations is much less clear. Most ice core studies attribute a change in methane

BGD
9, 13243–13286, 2012

concentration to a change in methane emissions from both boreal and sub-tropical to tropical wet ecosystems (Chappellaz et al., 1997; Fischer et al., 2008). The interpolar concentration gradient with higher values in the Northern versus the Southern Hemisphere during interstadials was reconstructed from ice core methane data from Greenland and Antarctica (Brook et al., 2000; Baumgartner et al., 2012). This gradient together with methane isotopic information indicates important sources during warm periods located in high northern latitudes (Bock et al., 2010). For the 8.2 kyr event, the interpolar gradient suggests that the CH_4 emissions must have been reduced in the early phase of the 8.2 kyr event in the Northern Hemisphere, followed by sub-tropical and tropical emission reductions (Spahni et al., 2003).

The dominant and most directly responding type of methane emitting ecosystems in the northern high latitudes, i.e. the latitudes with the strongest temperature response to rapid changes in the Atlantic Meridional Overturning Circulation (AMOC), are boreal peatlands (Dallenbach et al., 2000; Baumgartner et al., 2012). Northern high-latitude peatland and permafrost soils are associated with large carbon stocks that serve as a substrate for microbial methane production (Gorham, 1991; Roulet, 2000). For the understanding of the covariations of atmospheric methane and climate on abrupt events it is thus crucial to investigate the carbon cycle of northern high-latitude peatlands (northern peatlands hereafter). The carbon cycle response of northern peatlands is regulating the peatland methane emissions and thus directly affecting the global methane concentration within its atmospheric mixing and life time of ~ 2 and ~ 10 yr, respectively (Lelieveld et al., 1998; Denman et al., 2007; Prather, 2012). Accordingly, the goal of this study is to investigate how much of the CH_4 sensitivity to a rapid climate change can be explained by northern peatlands during the 8.2 kyr event.

There are two different attempts to model methane emissions from wet ecosystems for present day: bottom-up models that represent the processes leading to methane emissions in a mechanistic way (e.g. Cao et al., 1996; Walter et al., 2001; Wania et al., 2010; Ringeval et al., 2010) and top-down or inverse models which use observations of atmospheric methane concentrations and transport models to quantify

BGD
9, 13243–13286, 2012

methane emissions (e.g. Houweling et al., 1999; Pison et al., 2009; Bergamaschi et al., 2009). Combining both methods can help to narrow down the uncertainties of global wet ecosystem methane emissions (Spahni et al., 2011).

For past time periods, before the start of direct atmospheric methane monitoring in the 1980s, the spatially available CH_4 data is restricted to ice cores from Greenland and Antarctica and is not sufficient for applying top-down approaches. Accordingly, biogeochemical process modeling of methane emissions and comparisons of resulting atmospheric concentrations to ice core data is the only way to quantify natural methane emission distributions. Previous paleo-modeling studies have shown that simple methane models are capable of simulating emissions during abrupt events (van Huissteden, 2004; Hopcroft et al., 2011) and on long-term glacial-interglacial time scales (Valdes et al., 2005; Kaplan et al., 2006; Weber et al., 2010; Singarayer et al., 2011). The long-term simulations confirm the finding that atmospheric methane concentrations parallel temperature reconstructions from Antarctic ice cores also on glacial-interglacial time scales of the past 800 000 yr (Spahni et al., 2005; Loulergue et al., 2008). A drawback of previous paleo-modeling studies for methane is the limited representation of processes and interactions related to the interplay of vegetation and soil dynamics, soil temperature, soil hydrology, permafrost thawing, methane production, oxidation, and transport from the soils to the atmosphere by a variety of mechanisms. For example, Singarayer et al. (2011) and Kaplan et al. (2006) calculate the methane emissions as a fixed ratio of the heterotrophic respiration.

Here, we apply a process-oriented CH_4 module based on earlier work (Wania et al., 2009a,b, 2010) within the Bern version of the LPJ dynamic global vegetation model. Soil temperature at different depths, including freeze-thaw cycles, and water table position is explicitly calculated and CH_4 transport by soil diffusion, ebullition and through plant aerenchyma is simulated mechanistically. The focus of the study is on the 8.2 kyr event. For this period, the location of boreal peatlands is reasonably well known from recent observations, whereas modeling the response to DO events in the glacial would require a dynamical model of peat land development. Here we use present day boreal

BGD
9, 13243–13286, 2012

peatland distribution for the 8.2 kyr event. This approach appears to be justified, because comparison of the recent peat land distribution with the ice coverage 8200 yr ago (Peltier, 2004) shows that only very small areas of present day peatlands where covered by land ice at that time.

The outline of this paper is as follows. In Sects. 2.1 and 2.2, we describe the LPJ-Bern global dynamic vegetation model (Sitch et al., 2003; Joos et al., 2004; Gerber et al., 2003; Strassmann et al., 2008; Stocker et al., 2011), the implementation and improvements to LPJ-WHyMe (Wania et al., 2009a,b) and a recently developed methane module (Wania et al., 2010). Section 2.3 presents the calibration of the model with modern site data and describes the experimental setup for control simulations and for simulations forced with climate input from an ensemble of freshwater hosing model experiments (Bozbiyik et al., 2011). Results are presented in Sect. 3 and include simulated changes in CH_4 emissions for the set of freshwater hosing experiments, the attribution of change in CH_4 emissions to temperature and precipitation variations, and sensitivity on model parameters.

2 Model description and set-up

2.1 LPJ-Bern

The LPJ-Bern (hereafter LPJ) is a subsequent development of the Lund-Potsdam-Jena dynamic global vegetation model (LPJ-DGVM; Sitch et al., 2003) that combines process-based, large-scale representations of terrestrial vegetation dynamics and land-atmosphere carbon and water exchanges in a modular framework. Vegetation is defined by plant functional types (PFTs) each with its own set of parameters describing growth, carbon uptake and mortality. LPJ has been applied previously in paleo studies (e.g. Joos et al., 2004; Gerber et al., 2004) and in simulations assessing the anthropogenic climate perturbation and the impact of human induced landuse (e.g. Joos et al., 2001; Strassmann et al., 2008; Stocker et al., 2011).

BGD
9, 13243–13286, 2012

For this study we implemented the boreal peatland and methane module based on LPJ-WHyMe (Wetland Hydrology and Methane, Wania et al., 2009a,b, 2010) that derives its input data from the LPJ. It includes new features for grid cells with a (prescribed) partition of peatland: 8 soil layers, permafrost dynamics with freezing and thawing (including a soil temperature solver to simulate temperature as a function of depth), peatland hydrology (active layer depth and water table position), peatland vegetation as two additional PFTs (flood-tolerant C_3 graminoids and Sphagnum moss), a slow-down of decomposition under inundation and the addition of root exudates (Wania et al., 2009a,b).

The main scientific differences between our methane routine and the original LPJ-WHyMe version 1.3.1 (Wania et al., 2010) is a more mechanistic ebullition mechanism that includes also the partial pressure of CO_2 for triggering an ebullition event (see Sect. 2.2). The carbon balance over all layers is now preserved after every gas diffusion time step, whereas in LPJ-WHyMe the carbon balance was closed at the end of the year with a correction factor.

2.2 Methane routine in peatlands of LPJ-Bern

The carbon module simulates carbon allocation in vegetation, above and below ground litter and fast and slow soil carbon pools, as well as soil organic matter dynamics (Sitch et al., 2003). Heterotrophic respiration (HR) is calculated based on the size of the litter and soil pools, regulated by soil moisture and soil temperature at a depth of 25 cm. HR is then distributed to 8 peat layers according to the root distribution, where it is used to compute methane production. In each layer methane production is calculated as the product of HR, the ratio of CH_4 to CO_2 production under anaerobic conditions (f_{CH_4/CO_2}), and the anoxity of the soil for each soil layer (Wania et al., 2010).

Depending on the water table position, the soil temperature and the presence of O_2, the produced methane can be oxidised to CO_2, accumulated or transported to other layers or released to the atmosphere. The three implemented transport processes are plant-mediated transport, diffusion and ebullition. Plant-mediated transport

BGD
9, 13243–13286, 2012

is implemented as described in (Wania et al., 2010): the flood-tolerant C_3 graminoids (one of two PFTs growing in peatlands) are adapted to inundation by the presence of aerenchyma, gas-filled tissue, through which gas can be transported by diffusion. Plant-mediated transport depends on temperature, water content and the actual gradients of CH_4, CO_2 or O_2. The tiller radius r_{tiller} defines the open area available for plant-mediated transport and is a tunable parameter.

Diffusion transports O_2, CO_2 and CH_4 between the 8 soil layers. The temperature-dependent diffusion coefficients of all gases are set to their molecular diffusivities in air or water (Lerman, 1979; Broecker and Peng, 1974), depending on the water table position in the acrotelm (top 30 cm of soil). Peatland soil layers below that horizon are assumed to be completely water saturated (catotelm). Water can freeze if the soil layer temperature falls below 0 °C and all transport mechanisms are prohibited. CH_4 is not incorporated into the ice during freezing leading to an enrichment of CH_4 in the remaining water and an eventual release by ebullition.

The new ebullition mechanism calculates how much of the CH_4, CO_2 and N_2 is in the gas phase and how much is dissolved. Following Henry's law (FechnerLevy and Hemond, 1996; Rosenberry et al., 2003; Tokida et al., 2005, 2007) the amount of dissolved gases in each layer depends on partial pressure of CH_4, CO_2 and N_2, hydrostatic pressure, and soil temperature. The available volume ($V_{\text{available}}$) within each layer i is given by the layer thickness and the porosity for fully water saturated conditions. The total amount of N_2 is assumed to be constant, since it is not simulated by our model. However, the partitioning of N_2 between water and soil air changes. Assuming the gaseous volume of N_2 to be 1% (lower bound estimate, e.g. Shannon et al., 1996) of the available volume in a layer (liquid phase and gas phase), we calculate with Henry's law the amount of N_2 dissolved in each layer (Tokida et al., 2007). We then add the produced or transported CH_4 and CO_2 to the layer and recalculate the partial pressure for all gases (Eq. 1, Tokida et al., 2007; Kellner et al., 2006):

$$P_{x,i} = n_{x,i} R T_i \left(V_{\text{g},i} + \frac{V_{\text{w},i}}{H_x} \right)^{-1} \quad (1)$$

BGD
9, 13243–13286, 2012

where $P_{x,i}$ is the partial pressure of gas species x in layer i, $n_{x,i}$ is the total number of moles of gas x, $V_{g,i}$ is the gas volume, $V_{w,i}$ is the volume of liquid water, H_x is the dimensionless Henry's law constant for gas x (Yamamoto et al., 1976; Wiesenburg and Guinasso, 1979; Weiss, 1970), R is the universal gas constant, and T_i is the temperature in layer i (see Appendix). We assume that during ebullition the gas volume, $V_{g,i}$, is equal to 15 % and the liquid water volume, $V_{w,i}$, 85 % of the available volume (FechnerLevy and Hemond, 1996; Rosenberry et al., 2003; Tokida et al., 2005). In the code, ebullition is triggered if the sum of all partial pressures ($pN_2 + pCO_2 + pCH_4$) (Eq. 1 with $V_{g,i} = 15\,\% \cdot V_{available}$) is larger than the sum of atmospheric and hydrostatic pressure. The number of moles of CO_2 and CH_4 released per ebullition event is assumed to be 1 % of the available volume times the CO_2 and CH_4 partial pressure divided by $R\,T_i$, respectively. In other words, a fifteenth of the CO_2 and CH_4 amount in the gas phase is released per ebullition event. This assumption and that the gas volume is equal to 15 % of the available volume are not critical for the total emissions. Instead these parameters do modulate the frequency and the magnitude of ebullition events (see parameter tuning, Sect. 3.4).

Oxygen is transported into soils by diffusion through open soil pores and through the aerenchyma of the flood tolerant graminoids. Only a fraction (f_{oxid}) of the available oxygen is used to oxidise CH_4 to CO_2. The remaining O_2 is assumed to be consumed by other electron acceptors. Again f_{oxid} is a tunable model parameter.

2.3 Calibration and site validation

The implementation of LPJ-WHyMe into the LPJ-Bern, the code improvements and the adaption of the ebullition scheme calls for a re-evaluation of flux densities at the site level and a retuning of model parameters. We compare simulated CH_4 emissions to flux measurement at 7 sites. A detailed description of the sites and their environmental conditions can be found in Wania et al. (2010). Measured seasonal methane fluxes over a specific year are available for each site (Fig. 2) and (Bubier et al., 1998; Ding et al., 2004; Saarnio et al., 1997; Alm et al., 1999; Granberg et al., 2001; Johansson

BGD
9, 13243–13286, 2012

et al., 2006; Jackowicz-Korczynski et al., 2010; Shannon and White, 1994; Dise, 1993). We force LPJ with local temperature and precipitation for the sites in Abisko and Sanjiang and we use CRU-data (Climate Research Unit's (CRU) TS 2.1, climatology from 1901 to 2002, (New et al., 1999; Mitchell and Jones, 2005)) of the corresponding grid cell for the other sites for the calibration. LPJ is forced with monthly climate data, i.e. temperature (Fig. 4b), precipitation (Fig. 4c) and cloud cover, which are interpolated to daily values. The climate records include seasonal and interannual variability and are repeated over the spin-up period to reach a stable steady state.

The three most important factors for total methane emissions and the attribution to each emission pathway in the model turned out to be (i) the CH_4/CO_2-factor f_{CH_4/CO_2}, followed by (ii) the oxidation fraction f_{oxid} and (iii) the tiller radius r_{tiller} of peatland grasses. Other factors controling methane emissions are the exudate turnover rate, the moisture response, which is also used to calculate decomposition rates, the leaf-to-root ratio, which influences the cross-sectional area of aerenchyma available for plant-mediated gas transport, and the tiller porosity which influences the area for plant-mediated transport.

The CH_4/CO_2-factor, linking heterotrophic respiration and CH_4 production, directly affects the total production of CH_4 and thus total annual emissions. The oxidation fraction is the percentage of available O_2 that is used to oxidize CH_4 in each layer. Its effect is similar to the CH_4/CO_2-factor, but weaker. The tiller radius of peatland grasses influences directly the plant-mediated transport of O_2, CO_2 and CH_4. These three parameters were chosen to minimize the root mean square error between model results and data for the seven sites. Data and model results were smoothed using a spline approximation (Enting, 1987) with a cut-off period of two months. The spline covers the time period where the respective measurements exist. Nominally daily data were applied to compute that root mean square error for each site. The root mean square error for all sites is computed from the time period (spanned by measurements) weighted site errors. Local methane emissions for the best parameter set in this sensitivity study are shown in Fig. 2, together with the site measurements and the RMSE as computed

BGD
9, 13243–13286, 2012

from the spline fits. These optimized parameter set is then used to simulate global CH_4 emissions in the model experiment. The same set of parameters is used across all sites although a better fit with observational data could be achieved when parameters would be adjusted for each site individually. We find an improved agreement between model and observations compared to results presented by (Wania et al., 2010). This is likely related to the elimination of some coding errors and the improved representation of ebullition.

The optimized parameters are $0.17\,gC\,(gC)^{-1}$ for the ratio of CH_4/CO_2 production under anaerobic conditions, 0.5 for the oxidation fraction, i.e. the fraction of available oxygen used for methane oxidation, 0.0035 m for the tiller radius, and the assumption that ebullition occurs when 15 % of the available pore volume is gas and that 1 % of the available volume is released as gas in a single ebullition event. The influence of these parameters on modelled changes in methane emissions after a climate perturbation will be discussed in the result section.

It is possible to get similar root mean square deviations between model results and observations with different combinations for the production ratio and the oxidation fraction. Here, the oxidation factor is set as a standard to the same value (0.5) as in Wania et al. (2010). Very different fractions of oxygen consumption by methanogenesis have been reported, reaching from 0.2 to 1 (Wania, 2007; Frenzel and Rudolph, 1998; Strom et al., 2005). Changing parameters, governing plant-mediated transport or ebullition, changes the attribution to the different pathways, but does only weakly influence the total emission per unit area. To quantify the distribution better, either more site measurements would be needed or some further constraints like the ^{13}C signature of the total emissions.

Despite a rather well representation of the amplitide in CH_4 emissions in the course of the year a significant phase lag between observed and modelled CH_4 emissions is found for some sites as illustrated in Fig. 2. This may be partly attributed to the coarse resolution of the CRU data that drives the model for Boreas, Salmisuo, Degeroe, Michigan and Minnesota. In these cases CRU data are not necessarily representing the

BGD
9, 13243–13286, 2012

local conditions. For example a delayed rise in spring temperature leads to a time lag in soil thawing and thus methane production and emissions. Effects like water runoff from other regions are not taken into account either. However, the phase lag at Sanjiang, where site climate data were used, shows that also the seasonal change in the different emission processes is not accurately reflected by our model for all of the sites. The mismatch may be related to a possible neglect of heterotrophic respiration at shallow soils that thaw early in season. The methane routine distributes the total heterotrophic respiration that it gets as an input according to the root distribution and in case a layer is still frozen, the methane is put into the next unfrozen layer above. Analysis of the model output for Sanjiang shows that the soil thawing in deep layers has not began when the measured emissions start and the substrate for production is transferred to upper layers where it's almost completely oxidized.

Our sensitivity simulations presented in Sect. 3.4, show that also the partitioning between the different emission pathways (diffusion, plant transport, ebullition) has an influence on the seasonality of the emissions and is sensitive on the choice of model parameters, however the total annual emission is not. As illustrated in Fig. (3), the time-integrated CH_4 flux is well represented by the model across the different sites and a tight correlation ($R^2 = 0.92$) is found between simulated and measured cumulative site emissions. This indicates that the model has a good skill in representing annual emissions across a wide range of environmental conditions in the boreal zone. In conclusion, total annual emissions are simulated well across the different sites, while deviations between simulated and observed seasonal cycles remain (see also Wania, 2007).

2.3.1 Input data, spin-up, and setup for transient experiments

Spatially-resolved input data include the global land mask, the soil type (Zobler, 1986) (always "organic" on peatland) and a map of present day peatlands, here on a resolution of 3.75° longitude and 2.5° latitude. We prescribe the distribution and fraction of peatland area per grid cell (Tarnocai et al., 2009). The Tarnocai NCSCD data

BGD
9, 13243–13286, 2012

set (Tarnocai et al., 2007) includes histels and histosols that were rasterized and regridded to the model resolution (Fig. 4c), and scaled globally to match an area of 1048 million km^2 in the permafrost affected region in North America (Tarnocai et al., 2009). This scaling results in a Northern Hemisphere peatland area of 2.81 million km^2. This area is larger than the 2.06 million km^2 derived from the IGBP-DIS map as used in (Wania et al., 2010). Finally, input has to be provided for annual atmospheric CO_2 constant at 279 ppmv as found in ice cores for preindustrial conditions (Monnin et al., 2004) and the number of wet days per month (New et al., 1999; Mitchell and Jones, 2005).

LPJ is forced with monthly data of temperature (Fig. 4b), precipitation (Fig. 4c) and cloud cover. Here, climate output from a control run and a 3-member ensemble of freshwater hosing simulations recently conducted with the Climate System Model, version 1.4, (CSM1.4) of the National Centre for Atmospheric Research (NCAR) (Bozbiyik et al., 2011) is applied to simulate methane emissions and emission changes in northern peatlands during a cooling event similar to the 8.2 kyr event (Fig. 1). All CSM1.4 freshwater hosing simulations branch from the control simulations that features a stable climate and a constant freshwater input flux anomaly of 1 Sv (1 Sverdrup = 106 m^3 s^{-1}) is applied over 100 yr in the Northern North Atlantic. Freshwater input starts 126, 263, and 305 yr after the start of the control in ensemble simulation s1, s2, and s3 and simulations are continued for several centuries.

The monthly temperature and precipitation data of each CSM1.4 simulation are splined for each grid cell and each calendar month separately, using a 20-yr cut-off frequency (Enting, 1987) (Fig. 5). Anomalies for each month relative to the corresponding monthly mean of the CSM1.4 control run are computed. Monthly anomalies are then added to the CRU climatology (New et al., 1999; Mitchell and Jones, 2005). As the LPJ model is sensitive to the absolute input climatology, this procedure eliminates biases of the NCAR CSM 1.4 for modern climate relative to the CRU data set and, thus, corrects for climate-related biases in grid cell vegetation distribution and carbon stocks.

BGD
9, 13243–13286, 2012

All simulations are driven with a combination of the repeated 31-yr cycle of CRU data (TS 2.1, detrended climatology from 1960 to 1990, New et al., 1999; Mitchell and Jones, 2005) as a baseline and monthly anomalies from the NCAR CSM 1.4 model under preindustrial conditions. The spinup is done for all runs with the CRU climatology and the anomalies from the control run and is 1000 yr long. To accelerate the spin-up procedure, equilibrium soil carbon stocks are computed after 400 yr based on average input fluxes and decomposition rates. Then spin-up is continued for another 600 yr.

Simulated annual boreal methane emissions are scaled to 30 $Tg\,CH_4\,yr^{-1}$ for the end of the spinup period, which is a reasonable value for the present day and the preindustrial (Spahni et al., 2011, and therein). Since the area of effective methane emissions is highly heterogeneous, the simulated emissions have to be scaled accordingly. The prescribed peatland map only indicates the location of peat and the total area, but not its small scale structure. Peat layers on hummocks are emitting much less than peat layers in lawns. Accordingly, a perfect match of the total modeled peatland emission with best estimates from observations cannot be expected.

3 Results

3.1 Preindustrial emissions from boreal peatlands and interannual variability

Multi-year average methane emissions from peatlands are simulated to typically range between 0 to 50 $g\,C\,m^{-2}\,yr^{-1}$ (Fig. 7a) for the control. In general, emissions per unit area are relatively high in Northern Europe and in grid cells along the southern boundary of the peat zone in North America. Relatively low emissions per unit area are simulated in the Canadian Arctic and parts of Siberia, reflecting a generally short growing season and harsh climatic conditions (Fig. 4).

There is significant year-to-year climate variability and boreal methane emissions vary accordingly in the control simulation (Fig. 6). The range in annual emissions lies between 26 and 37 $Tg\,CH_4\,yr^{-1}$ and the standard deviation of annual emissions around

BGD
9, 13243–13286, 2012

the long-term mean is $\pm 1.8\,Tg\,CH_4\,yr^{-1}$ in the control. The spread in annual emission of 26 to $37\,Tg\,CH_4\,yr^{-1}$ may be compared with the spread of 29 to $37\,Tg\,CH_4\,yr^{-1}$ for Northern Hemisphere extratropical wetlands found by Chen and Prinn (2006) or 25 to $34\,Tg\,CH_4\,yr^{-1}$ by Spahni et al. (2011). Clearly, boreal wetland emissions have the potential to influence interannual variations in atmospheric methane by a few ppb.

3.2 Temporal and spatial changes in methane emissions after a climate perturbation

We next turn to the response for an 8.2 kyr-type event. The additional freshwater flux applied in the NCAR CSM1.4 ensemble simulations results in a collapse of the Atlantic Meridional Overturning Circulation and of the associated northward heat transport into the North Atlantic region with no sign of recovery until the end of the simulations. In turn, simulated temperature and precipitation in the North Atlantic and over the adjacent continents decrease relative to the stable CSM1.4 control run (Fig. 5). On annual and spatial average, using peatland area of each grid cell as weights, temperature over peatlands (40–90° N) decrease by about 2.5 °C within decades after adding the freshwater and remain low until the end of the simulations (Fig. 5c). Largest temperature anomalies over peatlands are simulated for the British Isles and Scandinavia, whereas simulated temperature changes remain small in Northern North America and the Siberian lowland, except in near-costal regions (Fig. 7a). Even a slight warming is simulated for the major peat regions in North America. On average, precipitation drops over peatland areas by 3 to 5 mm per month (Fig. 5d), with largest changes again in the British Isles (Fig. 7b). While the moss PFT was slightly dominant before the start of the freshwater input (foliar projective cover of 60 % for the moss PFT and 40 % for the grass PFT), it suffers more under the dryer and cooler conditions (50 % both afterwards). The biggest changes are in the Atlantic regions and the retreat of the sum of both PFTs is about 10 %.

BGD
9, 13243–13286, 2012

In response to the widespread decrease in temperature and precipitation, peatland CH_4 emissions are reduced by about 20 % compared to the control run. In accordance with the evolution of climate, emissions do not recover in the centuries after the perturbation (Fig. 6). These results are consistent across the three ensemble members. The spatial pattern of response reflects the change in climate with largest decrease in emissions per unit area of up to 25 $g C m^{-2} yr^{-1}$ in Northern Europe and small changes in Eastern North America and in the Siberian lowlands (Fig. 7b). A slight increase in emissions is even found South of Hudson Bay where an increase in temperature and small precipitation changes are simulated after the freshwater perturbation.

The decrease in emissions from boreal peatlands by 6 $Tg CH_4 yr^{-1}$ corresponds to a decrease of 18 ppb in atmospheric methane (assuming a lifetime of 8.4 yr Stevenson et al., 2006; Prinn, 1994; Lelieveld et al., 1998), and a unit conversion factor of 2.78 $Tg CH_4 ppbv^{-1}$. This decrease explains about 23 % of the 80 ppbv reduction during the 8.2 kyr event observed in ice core records (Fig. 1). This suggests that variations in emissions from boreal peatlands contributed significantly to the CH_4 variations recorded in ice cores, but that other boreal and especially tropical CH_4 sources varied as well.

3.3 Influence of changes in temperature and precipitation on emission changes

Next, we investigate the sensitivity of methane emission changes to changes in individual climatic drivers. This is done by factorial simulations where either precipitation anomalies or temperature anomalies from the NCAR CSM1.4 simulations are applied. The results show that the changes in the amount of precipitation and in temperature are about equally responsible for the drop in the total methane emissions from the northern peatlands (Fig. 8a); total emission decreases by about 4 $Tg CH_4 yr^{-1}$ in each simulation. The combined effect of temperature and precipitation is not the sum of the individual contributions to the CH_4 emission response. The main reason for this is that cells where the production and transport of methane is already inhibited by low temperatures cannot further be reduced in their activity by missing water and vice versa,

BGD
9, 13243–13286, 2012

grid cells with no activity due to too dry conditions are inactive independent of a further decrease in temperature. In conclusion, both temperature and precipitation changes influence CH_4 emissions significantly.

3.4 Governing processes and their sensitivity to model parameters

We now turn our attention to the importance of individual processes for methane emissions from boreal peatlands. Gross primary productivity (GPP) by the two plant functional types existing on boreal peatlands decreases by 14 % from 1463 to 1258 $Tg\,C\,yr^{-1}$ after the freshwater input, net primary productivity (NPP) by 12 % from 839 to 739 Tg C and total (aerobic and anaerobic) heterotrophic respiration (HR) by 13 % from 837 to 731 Tg C. This decrease is driven by the general decrease in temperature and precipitation in about equal parts as inferred from the factorial simulations described above. In turn, the simulated total soil carbon inventory in boreal peatlands of 536 Pg C, including the litter above and below ground, the exudates, and a fast and a slowly decaying soil carbon pool, remains virtually unchanged (532 Pg C). The decrease in respiration is thus the result of a decrease in the mean decomposition rate of organic material and not of a decrease in soil carbon inventory. Note that the soil carbon inventory which is in steady state and under preindustrial conditions is realistic compared to available data (MacDonald et al., 2006) and therefore also higher than at the beginning of the 8.2 kyr event. The average yearly water table position over all peatland gridcells drops from 4 mm below the surface to 6 mm. The biggest changes are in the Atlantic regions and the adjacent areas with up to 110 mm change in the annual mean.

In our model, production of methane is linearly scaled with the rate of heterotrophic respiration and total preindustrial emissions from peatlands are scaled to 30 $Tg\,CH_4\,yr^{-1}$ as described in the method section. For the standard set of parameters, preindustrial total methane production amounts to 41.9 $Tg\,CH_4\,yr^{-1}$ of which 28 % (11.7 $Tg\,CH_4\,yr^{-1}$) are removed within the soil by oxidiation. After the freshwater

BGD
9, 13243–13286, 2012

pulse, production drops on average to 35.4 Tg CH_4 yr^{-1} of which again about 30 % (10.7 Tg CH_4 yr^{-1}) are oxidized and 70 % emitted (Fig. 8a). The bottom line of this is that 2.7 % of total NPP and HR is converted into methane (22.5 Tg C/839 Tg C and 22.5 Tg C/837 Tg C) under preindustrial conditions. However, these fractions drop to 2.5 % under the climate prevailing after the freshwater input. This suggests that a fixed scaling of CH_4 emissions to total heterotrophic respiration may not be adequate to simulate variations in CH_4 emissions under varying climate conditions such as reconstructed for Dansgaard-Oeschger events or glacial-interglacial cycles.

The total methane emission flux is the sum of plant transport, diffusion and ebullition. For the standard parameter choice, ebullition and plant transport are the dominant transport pathways (solid lines in Fig. 8b) and each contribute about 35 to 40 % to the total emission. The percentage contribution of these pathways to total emissions remains roughly constant after the climatic perturbation. The fraction of methane that is oxidized remains also fairly constant.

Next, we analyse the sensitivity of the simulated emissions and their changes to the choice of model parameters in the methane module (Table 1). In a suite of sensitivity experiments, a parameter is varied individually around its standard value. Each run is rescaled with the same factor that scales the standard parameters run to 30 Tg CH_4 yr^{-1} at the end of the spin-up. Parameters varied are the CH_4/CO_2 production factor, the oxidation factor, i.e. the percentage of available O_2 that is used to oxidize CH_4 in each layer, and the tiller radius of the peatland grass PFT and the two parameters controlling the ebullition mechanism.

The CH_4/CO_2 production factor and the oxidation fraction (range 0.2 to 0.6) scale the total methane emissions from boreal wetlands almost linearly under preindustrial conditions. Changing the parameters governing methane transport to reduce a specific methane emission pathway usually leads to an increased flux by the other two pathways as a compensation. However, large reductions in emissions through one pathway are only partially compensated. For illustration Fig. 8b shows a comparison between the standard run and a run with a doubled tiller radius. As shown by Wania et al. (2010),

BGD
9, 13243–13286, 2012

an increase in the tiller radius leads to more plant-mediated transport and in turn to a lower ebullition flux (Fig. 8b), whereas the diffusive flux to the atmosphere remains practically unchanged. A larger tiller radius increases O_2 diffusion into the soil, and thus potentially favours oxidation. At the same time, a larger tiller radius also favours a larger methane efflux to the atmosphere (Wania et al., 2010). We find that the fraction of produced methane that is oxidized in the soil increases from 30 to 32 % when the tiller radius is doubled.

It is interesting to analyse how the drop in emission for an 8.2 kyr-type climate anomaly depends on the choice of parameters. The reduction in methane emissions after the freshwater perturbation does barely depend on the oxidation fraction (Table 1). The reduction in emissions in only 16.9 % when the oxidation fraction is set to 0.2 compared to a reduction by −18.6 % for the standard value of 0.5. Correspondingly, the reduction in emissions becomes slightly larger if a larger fraction of available oxygen is used for methane oxidation. Changes in the tiller radius and in the parameters governing ebullition have as well a small influence on the simulated change in emission (Table 1).

4 Conclusions

Various climate input scenarios and parameter sets were used to model methane emissions during a freshwater experiment under interglacial climate conditions, reflecting conditions similar to the 8.2 kyr event. The result that methane emissions from northern peatlands drop during an average monthly precipitation change of 3 mm and an average temperature drop of about 2.5 °C over 50 yr by 20 % is generally insensitive to the parameter selection. The driving factor for the magnitude of the modelled emissions is the production. Changes in the parameters that describe the different transport mechanisms influence the seasonal timing of the emissions and the attribution to the different pathways on grid cell basis, but do not change the global emission signal significantly. When temperature and water content are in an ideal range, methane is

BGD
9, 13243–13286, 2012

produced and gets steadily transported to layers with less methane concentration, directly to the atmosphere or gets stored in the soil. In the latter case it stays until it reaches the threshold for ebullition, which is the fastest and most efficient transport way.

CH_4 production also changes significantly from year to year in our model. The modeled inter-annual variability in CH_4 emissions is on the order of $10\,Tg\,CH_4\,yr^{-1}$, which is comparable to the variability found by Chen and Prinn (2006) or Spahni et al. (2011). This inter-annual variability amounts to a third of the average peatland emissions of $30\,Tg\,CH_4\,yr^{-1}$ and is also comparable in size to the average decline in CH_4 emissions found during our freshwater hosing experiment. Accordingly, the decline in peatland CH_4 emissions during the freshwater hosing event in our model is caused by a direct, fast response of the existing peatland ecosystems on the occuring climate change. The observed emission decline during the freshwater hosing experiment also occurs on time scales of years to decades, again showing that existing peatlands are able to respond quickly and sensitively to changing climate boundary conditions in our model. Thus, a change in peatland emissions on the order of $10\,Tg\,CH_4\,yr^{-1}$ does not require a much slower climate induced geographical relocation of peatlands or a change in peatland ecosystem structure, such as a transgression from fens to bogs. Note, that such a dynamic relocation or aging of peatlands is not yet included in our model, but would become important for the simulation of glacial CH_4 emissions or during transient Holocene climate conditions on time scales of millenia, where peatland location and ecosystem composition can change. E.g. during glacial times northern boreal wetlands have most likely been displaced southwards in response to the widespread cooling. Peatland distribution (and peatland ecosystem structure) may have also somewhat different for the time interval 8200 yr ago, when some ice remnants still existed in North America (Peltier, 1994). However, only a few grid cells of modern peat occurrence were still ice covered and warm Holocene climate conditions prevailed already for more than 1000 yr at that time allowing for a relaxation of peat distribution to interglacial conditions. For the 8.2 kyr event itself, which lasted only about 150 yr, a peatland relocation in

BGD
9, 13243–13286, 2012

response to the cooling appears to be unlikely as the time scale for peat development is much longer (Weber et al., 2010).

Assuming total emissions of 30 Tg CH_4 yr^{-1}, the emission change during the cooling event explains a variation in the atmospheric methane concentration of about 18 ppbv. Taken at face value this cannot quantitatively explain the 80 ppbv change found in ice cores during the 8.2 kyr event. Accordingly other sources such as tropical wetlands, but also other boreal and mid-latitude sources are likely to be affected by the 8.2 kyr event. However, scaling the annual average emissions to 30 Tg CH_4 yr^{-1} directly determines the magnitude of the emission reduction and thus of the implied decrease in atmospheric CH_4.

Total average CH_4 emissions of 30 Tg CH_4 yr^{-1} correspond to results from Spahni et al. (2011), compatible with Chen and Prinn (2006) and MacDonald et al. (2006) for current conditions, but is at the lower end compared to the survey of Zhuang et al. (2004). Zhuang et al. (2004) summarized the recent literature and found that emission estimates for the pan-arctic region from eleven studies ranged from 31 to 106 Tg CH_4 yr^{-1} although the upper end of their range is incompatible with ice core observations on the interhemispheric CH_4 gradient (Brook et al., 2000; Baumgartner et al., 2012). MacDonald et al. (2006) also suggests that boreal wetland CH_4 emissions might have been higher at 8 kyr BP than today although peat extent was lower. The reason for this is that the emissions from minerotrophic fens that dominated early during peat formation are much higher than from the currently predominant ombrotrophic sphagnum bogs that only developed over time. They suggest that the northern peatland complex was likely at 20 % of its current aerial extent at the end of the YD and expanded to about 50 % by 8 ka. On the basis of current estimates of overall CH_4 production from northern peatlands, they may have contributed up to 12 to 27 Tg CH_4 yr^{-1} by 8 ka. However, taking the higher CH_4 emission rates of early fens into account MacDonald et al. (2006) speculate that the emissions before the 8.2 kyr event may have been also considerably larger. Accordingly this would then also imply a larger drop in CH_4 concentrations during the 8.2 kyr event.

BGD
9, 13243–13286, 2012

Brook et al. (2000) and Baumgartner et al. (2012) estimate the total CH_4 source strength in the Northern Hemisphere to be 60–70 $Tg\,CH_4\,yr^{-1}$ for the early Holocene. This estimate includes all extratropical CH_4 sources (e.g. ruminants, wet soils, thawing of submerged permafrost, thermokarst lakes etc, where thermokarst lakes alone are estimated to account for up to 15 $Tg\,CH_4\,yr^{-1}$ but could be taken as an upper boundary. If we set the annual average peatland emissions to 50 instead of 30 $Tg\,CH_4\,yr^{-1}$, we could explain a 30 ppbv change during our freshwater hosing experiment. This could still only explain about 40 % of the observed CH_4 decrease during the 8.2 kyr event. Accordingly, a substantial contribution of tropical and other boreal sources to this event remains most likely.

Although our findings are generally within the range of other estimates and ice core observations, they are still subject to considerable uncertainties both with respect to the total peatland CH_4 emissions as well as the processes on the soil and ecosystem level. To constrain the parameters further, additional information from field data and potentially from isotopic information are required. Moreover temporal changes also exist in the CH_4 emissions of peatland ecosystems. As outlined above the temporal transgression of peatlands from minerotrophic fens to ombrotrophic bogs is not yet included in our model. Sowers (2010) measured a decreasing trend in $\delta^{13}C$ throughout the Holocene beginning at −46.4 permil at 11 kyr BP and decreasing to −48.4 permil at 1 ka. They suggest the 2 permil $\delta^{13}C$ drop is likely to be a combination of increased CH_4 emissions from Arctic lakes and wetlands, an increase in the ratio of C_3/C_4 plants in wetlands and an increase in methanogenic communities utilizing the CO_2 reduction pathway as compared to the acetate fermentation pathway. In particular the latter process would be directly related to the transgression of fens to bogs and could explain the $\delta^{13}CH_4$ shift observed in ice cores (Sowers, 2010) in the first half of the Holocene.

Generally, model improvements could be made for example by a carbon allocation to the different layers instead of an overall total number for HR given to the methane routine, a more sophisticated parametrisation of the soil anoxity that regulates the production, a changing ratio of CH_4 production and HR in transient simulations (possible

BGD
9, 13243–13286, 2012

implication for simple models) and by including a dynamic peatland distribution. The simulations done for this study could be improved by choosing more specific boundary conditions for the 8.2 kyr event (such as an improved peatland distribution map, the climate influence of the ice sheet remnants and the choice of orbital parameters and CO_2 concentrations at the time of the 8.2 kyr event) instead of preindustrial conditions as used in these simulations. There are also uncertainties to which extend the NCAR climate input is appropriate to do a 8.2 kyr event like simulation. To improve the model calibration more site measurements would be needed and some further constraints like the ^{13}C signature would give additional constraints for the attribution to the different processes.

Appendix A

Ebullition routine

We assume the existence of three gas species CH_4, $CO_2$and N_2 in the bubbles (Tokida et al., 2007). All calculations are done for each soil layer separately.

x	gas species (CH_4, CO_2, N_2)
$V_{available}$	available volume (liquid and gas bubbles, not frozen) in a layer per m^2 (m)
V_{gas}	total gas volume per m^2 (m)
$V_{diss,x}$	dissolved volume of species x per m^2 (m)
V_{diss}	volume in which the gases can dissolve per m^2 (m)
V_{ice}	frozen volume in a layer per m^2 (m)
ρ	porosity
T	temperature in a layer (°C)
R	universal gas constant
D_z	thickness of layer z (m)
P_E	pressure at depth of layer z (Pa)

BGD
9, 13243–13286, 2012

H_x dimensionless Henry constant (ratio of aqueous to gaseous phase) for gas x
n_x total number of moles of gas species x per m^2 ($mol\,m^{-2}$)
$V_{gas,\ ebull}$ gas volume at threshold o ebullition (m)
$P_{gas,x}$ partial pressure of gas species x (Pa)
P_{gas} gas pressure (Pa)
ΔV total gas volume lost through an ebullition event per m^2 (m)
Δn_x change in total amount of gas species x ($mol\,m^{-2}$)
Δm_x total mass change in gas species x ($g\,m^{-2}$)
M_x molar mass of gas species x ($g\,mol^{-1}$)

The available space per m^2, $V_{available}$, is the layer height multiplied by the porosity and corrected for the frozen volume.

$$V_{available} = V_{gas} + V_{diss} = \rho \cdot D_z - V_{ice} (m^3\,m^{-2}) \quad \text{(A1)}$$

The soil in wetlands is divided in the acrotelm (defined as the upper 0.3 m which experiences a fluctuating water table) and the catotelm, the underlying permanently inundated layers with 1.7 m thickness. The respective porosities are $\rho_{acro} = 0.9$ for the three first layers, $\rho_{cato} = 0.8$ for the 5 deeper layers.

P_E is the environmental pressure and therefore the sum of the atmospheric pressure (101 325 Pa) and the hydrostatic pressure.

Initial conditions:

$$n_{CO_2} = n_{CH_4} = 0 \quad \text{(A2)}$$

$$V_{gas} = 1\,\% V_{available} \quad \text{(A3)}$$

$$V_{diss,N_2} = 99\,\% V_{available} \quad \text{(A4)}$$

BGD
9, 13243–13286, 2012

We assume the gaseous volume of N_2 to be 1% (see Sect. 2.3) of the available volume. With Eq. (1) (ideal gas law and mass balance) we can calculate the total amount of N_2

$$n_{N_2} = \frac{P_E \cdot (V_{gas} + \frac{V_{diss}}{H_{N_2}})}{RT} (\mathrm{mol\,m^{-2}}) \quad \text{(A5)}$$

Now we add CH_4 and CO_2 as they are simulated in the model.

$$n_{CO_2}(t) = n_{CO_2}(t-1) + \Delta n_{CO_2} \quad \text{(A6)}$$

$$n_{CH_4}(t) = n_{CH_4}(t-1) + \Delta n_{CH_4} \quad \text{(A7)}$$

For the ebullition criterion we assume that it is critical if the gas volume exceeds 15% of the available volume

$$V_{gas} \geq 15\% V_{available} \quad \text{(A8)}$$

and compute $P_{gas,x}$.

$$P_{gas,x} = \frac{n_x RT}{V_{gas} + \frac{V_{diss}}{H_x}} = \frac{n_x RT}{15\% V_{available} + \frac{85\% V_{available}}{H_x}} \quad \text{(A9)}$$

If $P_{gas} \geq P_E$, ebullition is triggered:

$$P_{gas} = \sum_x P_{gas,x} \geq P_E \quad \text{(A10)}$$

We assume that a fifteenth of the total gas volume bubbles out. The assumption is not critical (see Sect. 3.4)

$$\Delta V = 1\% V_{available} \quad \text{(A11)}$$

BGD
9, 13243–13286, 2012

Therefore, the change in the total amount of CO_2 and CH_4 is

$$\Delta n_x = \frac{\Delta V P_x}{RT} (\mathrm{mol\,m^{-2}}) \quad \text{(A12)}$$

$$\Delta m_x = \Delta n_x \cdot M_x (\mathrm{g\,m^{-2}}) \quad \text{(A13)}$$

while n_{N_2} is kept constant.

Acknowledgements. Financial support for this study was provided by the European Research Council advanced grant MATRICs (ERC grant agreement no. 226172) under the European Community's Seventh Framework Programme. We appreciate support by the Swiss National Science Foundation through the National Centre of Competence in Research (NCCR) Climate and its grant of the Division of Climate and Environmental Physics, and by the European Commission through the FP7 project Past4Future (grant no. 243908).

References

Alm, J., Saarnio, S., Nykanen, H., Silvola, J., and Martikainen, P.: Winter CO_2, CH_4 and N_2O fluxes on some natural and drained boreal peatlands, Biogeochemistry, 44, 163–186, doi:10.1023/A:1006074606204, 1999. 13251

Baumgartner, M., Schilt, A., Eicher, O., Schmitt, J., Schwander, J., Spahni, R., Fischer, H., and Stocker, T. F.: High-resolution interpolar difference of atmospheric methane around the Last Glacial Maximum, Biogeosciences Discuss., 9, 5471–5508, doi:10.5194/bgd-9-5471-2012, 2012. 13245, 13246, 13263, 13264

Bergamaschi, P., Frankenberg, C., Meirink, J. F., Krol, M., Villani, M. G., Houweling, S., Dentener, F., Dlugokencky, E. J., Miller, J. B., Gatti, L. V., Engel, A., and Levin, I.: Inverse modeling of global and regional CH_4 emissions using SCIAMACHY satellite retrievals, J. Geophys. Res., 114, D22301, doi:10.1029/2009JD012287, 2009. 13247

Blunier, T. and Brook, E.: Timing of millennial-scale climate change in Antarctica and Greenland during the last glacial period, Science, 291, 109–112, doi:10.1126/science.291.5501.109, 2001. 13245

BGD
9, 13243–13286, 2012

Blunier, T., Chappellaz, J., Schwander, J., Stauffer, B., and Raynaud, D.: Variations in atmospheric methane concentration during the holocene epoch, Nature, 374, 46–49, doi:10.1038/374046a0, 1995. 13245

Bock, M., Schmitt, J., Moeller, L., Spahni, R., Blunier, T., and Fischer, H.: Hydrogen isotopes preclude marine hydrate CH_4 emissions at the onset of Dansgaard-Oeschger events, Science, 328, 1686–1689, doi:10.1126/science.1187651, 2010. 13246

Bozbiyik, A., Steinacher, M., Joos, F., Stocker, T. F., and Menviel, L.: Fingerprints of changes in the terrestrial carbon cycle in response to large reorganizations in ocean circulation, Clim. Past, 7, 319-338, doi:10.5194/cp-7-319-2011, 2011. 13248, 13255

Broecker, W. and Peng, T.: Gas-exchange rates between air and sea, Tellus, 26, 21–35, 1974. 13250

Brook, E., Harder, S., Severinghaus, J., Steig, E., and Sucher, C.: On the origin and timing of rapid changes in atmospheric methane during the last glacial period, Global Biogeochem. Cy., 14, 559–572, doi:10.1029/1999GB001182, 2000. 13245, 13246, 13263

Bubier, J. L., Crill, P. M., Varner, R. K. and Moore, T. R. BOREAS TGB-01/TGB-03 CH4 chamber flux data: NSA Fen. Data set, available online: http://www.daac.ornl.gov from Oak Ridge National Laboratory Distributed Archive Center, Technical report, Oak Ridge, Tennessee, USA, last access date: 24 September, 2012 (access date: September 2012), 1998. 13251

Cao, M., Marshall, S., and Gregson, K.: Global carbon exchange and methane emissions from natural wetlands: application of a process-based model, J. Geophys. Res., 101, 14399–14414, doi:10.1029/96JD00219, 1996. 13246

Chappellaz, J., Blunier, T., Raynaud, D., Barnola, J., Schwander, J., and Stauffer, B.: Synchronous changes in atmospheric CH_4 and Greenland climate between 40-KYR AND 8-KYR BP, Nature, 366, 443–445, doi:10.1038/366443a0, 1993. 13245

Chappellaz, J., Blunier, T., Kints, S., Dallenbach, A., Barnola, J., Schwander, J., Raynaud, D., and Stauffer, B.: Changes in the atmospheric CH_4 gradient between Greenland and Antarctica during the Holocene, J. Geophys. Res., 102, 15987–15997, doi:10.1029/97JD01017, 1997. 13245, 13246

Chen, Y.-H. and Prinn, R. G.: Estimation of atmospheric methane emissions between 1996 and 2001 using a three-dimensional global chemical transport model, J. Geophys. Res., 111, D10307, doi:10.1029/2005JD006058, 2006. 13257, 13262, 13263

Dallenbach, A., Blunier, T., Fluckiger, J., Stauffer, B., Chappellaz, J., and Raynaud, D.: Changes in the atmospheric CH_4 gradient between Greenland and Antarctica during the

BGD
9, 13243–13286, 2012

Last Glacial and the transition to the Holocene, Geophys. Res. Lett., 27, 1005–1008, doi:10.1029/1999GL010873, 2000. 13246

Denman, K. L., Brasseur, G., Chidthaisong, A., Ciais, P., Cox, P., Dickinson, R. E., Hauglustaine, D., Heinze, C., Holland, E., Jacob, D., Lohmann, U., Ramachandran, S., da Silva Dias, P. L., Wofsy, S. C., and Zhang, X.: Chapter 7: Couplings between changes in the climate system and biogeochemistry, in: Climate Change 2007: The Physical Science Basis. Contribution of Working Group I to the Fourth Assessment Report of the Intergovernmental Panel on Climate Change, edited by: Solomon, S., Qin, D., Manning, M., Chen, Z., Marquis, M., Averyt, K., Tignor, M., and Miller, H., Cambridge Univ. Press, UK and New York, NY, USA, 499–588, 2007. 13246

Ding, W., Cai, Z., and Wang, D.: Preliminary budget of methane emissions from natural wetlands in China, Atmos. Environ., 38, 751–759, doi:10.1016/j.atmosenv.2003.10.016, 2004. 13251

Dise, N.: Methane emission from Minnesota peatlands – spatial and seasonal variability, Global Biogeochem. Cy., 7, 123–142, doi:10.1029/92GB02299, 1993. 13252

Dlugokencky, E., Bruhwiler, L., White, J., Emmons, L., Novelli, P., Montzka, S., Masarie, K., Lang, P., Crotwell, A., Miller, J., and Gatti, L.: Observational constraints on recent increases in the atmospheric CH_4 burden, Geophys. Res. Lett., 36, L18803, doi:10.1029/2009GL039780, 2009. 13245

Ellison, C., Chapman, M., and Hall, I.: Surface and deep ocean interactions during the cold climate event 8200 years ago, Science, 312, 1929–1932, doi:10.1126/science.1127213, 2006. 13245

Enting, I.: On the use of smoothing splines to filter CO_2 data, J. Geophys. Res., 92, 10977–10984, doi:10.1029/JD092iD09p10977, 1987. 13252, 13255

FechnerLevy, E. and Hemond, H.: Trapped methane volume and potential effects on methane ebullition in a northern peatland, Limnol. Oceanogr., 41, 1375–1383, 1996. 13250, 13251

Fischer, H., Behrens, M., Bock, M., Richter, U., Schmitt, J., Loulergue, L., Chappellaz, J., Spahni, R., Blunier, T., Leuenberger, M., and Stocker, T. F.: Changing boreal methane sources and constant biomass burning during the last termination, Nature, 452, 864–867, doi:10.1038/nature06825, 2008. 13246

Flückiger, J., Blunier, T., Stauffer, B., Chappellaz, J., Spahni, R., Kawamura, K., Schwander, J., Stocker, T., and DahlJensen, D.: N_2 and CH_4 variations during the last glacial epoch: insight

BGD
9, 13243–13286, 2012

into global processes, Global Biogeochem. Cy., 18, GB1020, doi:10.1029/2003GB002122, 2004. 13245
Frenzel, P. and Rudolph, J.: Methane emission from a wetland plant: the role of CH_4 oxidation in Eriophorum, Plant Soil, 202, 27–32, doi:10.1023/A:1004348929219, 1998. 13253
Gerber, S., Joos, F., Brugger, P., Stocker, T., Mann, M., Sitch, S., and Scholze, M.: Constraining temperature variations over the last millennium by comparing simulated and observed atmospheric CO_2, Clim. Dyn., 20, 281–299, doi:10.1007/s00382-002-0270-8, 2003. 13248
Gerber, S., Joos, F., and Prentice, I. C.: Sensitvity of a dynamic global vegetation model to climate and atmospheric CO_2, Global Change Biol., 10, 1223–1239, 2004. 13248
Gorham, E.: Northern peatlands – role in the carbon-cycle and probable responses to climatic warming, Ecol. Appl., 1, 182–195, doi:10.2307/1941811, 1991. 13246
Grachev, A. M. and Severinghaus, J. P.: A revised $+10 \pm 4\,^{\circ}C$ magnitude of the abrupt change in Greenland temperature at the Younger Dryas termination using published GISP2 gas isotope data and air thermal diffusion constants, Quat. Sci. Rev., 24, 513–519, doi:10.1016/j.quascirev.2004.10.016, 2005. 13245
Granberg, G., Ottosson-Lofvenius, M., Grip, H., Sundh, I., and Nilsson, M.: Effect of climatic variability from 1980 to 1997 on simulated methane emission from a boreal mixed mire in Northern Sweden, Global Biogeochem. Cy., 15, 977–991, doi:10.1029/2000GB001356, 2001. 13251
Hopcroft, P. O., Valdes, P. J., and Beerling, D. J.: Simulating idealized Dansgaard-Oeschger events and their potential impacts on the global methane cycle, Quat. Sci. Rev., 30, 3258–3268, doi:10.1016/j.quascirev.2011.08.012, 2011. 13247
Houweling, S., Kaminski, T., Dentener, F., Lelieveld, J., and Heimann, M.: Inverse modeling of methane sources and sinks using the adjoint of a global transport model, J. Geophys. Res., 104, 26137–26160, 1999. 13247
Huber, C., Leuenberger, M., Spahni, R., Fluckiger, J., Schwander, J., Stocker, T., Johnsen, S., Landals, A., and Jouzel, J.: Isotope calibrated Greenland temperature record over Marine Isotope Stage 3 and its relation to CH_4, Earth Planet. Sc. Lett., 243, 504–519, doi:10.1016/j.epsl.2006.01.002, 2006. 13245
Jackowicz-Korczynski, M., Christensen, T. R., Backstrand, K., Crill, P., Friborg, T., Mastepanov, M., and Strom, L.: Annual cycle of methane emission from a subarctic peatland, J. Geophys. Res.-Biogeosci., 115, G02009, doi:10.1029/2008JG000913, 2010. 13252

BGD
9, 13243–13286, 2012

Johansson, T., Malmer, N., Crill, P. M., Friborg, T., Akerman, J. H., Mastepanov, M., and Christensen, T. R.: Decadal vegetation changes in a northern peatland, greenhouse gas fluxes and net radiative forcing, Global Change Biol., 12, 2352–2369, doi:10.1111/j.1365-2486.2006.01267.x, 2006. 13251

Joos, F., Prentice, I. C., Sitch, S., Meyer, R., Hooss, G., Plattner, G.-K., Gerber, S., and Hasselmann, K.: Global warming feedbacks on terrestrial carbon uptake under the Intergovernmental Panel on Climate Change (IPCC) emission scenarios, Global Biogeochem. Cy., 15, 891–907, 2001. 13248

Joos, F., Gerber, S., Prentice, I., Otto-Bliesner, B., and Valdes, P.: Transient simulations of Holocene atmospheric carbon dioxide and terrestrial carbon since the Last Glacial Maximum, Global Biogeochem. Cy., 18, GB2002, doi:10.1029/2003GB002156, 2004. 13248

Kaplan, J. O., Folberth, G., and Hauglustaine, D. A.: Role of methane and biogenic volatile organic compound sources in late glacial and Holocene fluctuations of atmospheric methane concentrations, Global Biochem. Cy., 20, GB2016, doi:10.1029/2005GB002590, 2006. 13247

Kellner, E., Baird, A. J., Oosterwoud, M., Harrison, K., and Waddington, J. M.: Effect of temperature and atmospheric pressure on methane (CH_4) ebullition from near-surface peats, Geophys. Res. Lett., 33, L18405, doi:10.1029/2006GL027509, 2006. 13250

Kobashi, T., Severinghaus, J. P., Brook, E. J., Barnola, J.-M., and Grachev, A. M.: Precise timing and characterization of abrupt climate change 8200 years ago from air trapped in polar ice, Quat. Sci. Rev., 26, 1212–1222, doi:10.1016/j.quascirev.2007.01.009, 2007. 13245, 13279

Lelieveld, J., Crutzen, P., and Dentener, F.: Changing concentration, lifetime and climate forcing of atmospheric methane, Tellus B, 50, 128–150, doi:10.1034/j.1600-0889.1998.t01-1-00002.x, 1998. 13246, 13258

Lerman, A.: Geochemical Processes: Water and Sediment Environments, Wiley, New York, 1979. 13250

Loulergue, L., Schilt, A., Spahni, R., Masson-Delmotte, V., Blunier, T., Lemieux, B., Barnola, J.-M., Raynaud, D., Stocker, T. F., and Chappellaz, J.: Orbital and millennial-scale features of atmospheric CH_4 over the past 800 000 years, Nature, 453, 383–386, doi:10.1038/nature06950, 2008. 13245, 13247

MacDonald, G. M., Beilman, D. W., Kremenetski, K. V., Sheng, Y., Smith, L. C., and Velichko, A. A.: Rapid early development of circumarctic peatlands and atmospheric CH_4

BGD
9, 13243–13286, 2012

and CO_2 variations, Science, 314, 285–288, doi:10.1126/science.1131722, 2006. 13259, 13263
McManus, J., Francois, R., Gherardi, J., Keigwin, L., and Brown-Leger, S.: Collapse and rapid resumption of Atlantic meridional circulation linked to deglacial climate changes, Nature, 428, 834–837, doi:10.1038/nature02494, 2004. 13245
Mitchell, T. D. and Jones, P. D.: An improved method of constructing a database of monthly climate observations and associated high-resolution grids, Int. J. Climatol., 25, 693–712, doi:10.1002/joc.1181, 2005. 13252, 13255, 13256, 13282
Monnin, E., Steig, E., Siegenthaler, U., Kawamura, K., Schwander, J., Stauffer, B., Stocker, T., Morse, D., Barnola, J., Bellier, B., Raynaud, D., and Fischer, H.: Evidence for substantial accumulation rate variability in Antarctica during the Holocene, through synchronization of CO_2 in the Taylor Dome, Dome C and DML ice cores, Earth and Planet. Sci. Lett., 224, 45–54, doi:10.1016/j.epsl.2004.05.007, 2004. 13255
New, M., Hulme, M., and Jones, P.: Representing twentieth-century space-time climate variability. Part I: Development of a 1961–90 mean monthly terrestrial climatology, J. Climate, 12, 829–856, 1999. 13252, 13255, 13256, 13282
Peltier, W.: Ice-age paleotopography, Science, 265, 195–201, doi:10.1126/science.265.5169.195, 1994. 13262
Peltier, W.: Global glacial isostasy and the surface of the ice-age Earth: the ICE-5G (VM2) model and GRACE, Annu. Rev. Earth Pl. Sc., 32, 111–149, 2004. 13248
Pison, I., Bousquet, P., Chevallier, F., Szopa, S., and Hauglustaine, D.: Multi-species inversion of CH_4, CO and H_2 emissions from surface measurements, Atmos. Chem. Phys., 9, 5281–5297, doi:10.5194/acp-9-5281-2009, 2009. 13247
Prather, M. J., Holmes, C. D., and Hsu, J.: Reactive greenhouse gas scenarios: systematic exploration of uncertainties and the role of atmospheric chemistry, Geophys. Res. Lett., 39, L09803, doi:10.1029/2012GL051440, 2012. 13246
Prinn, R.: The interactive atmosphere – global atmospheric-biospheric chemistry, Ambio, 23, 50–61, 1994. 13258
Ringeval, B., de Noblet-Ducoudre, N., Ciais, P., Bousquet, P., Prigent, C., Papa, F., and Rossow, W. B.: An attempt to quantify the impact of changes in wetland extent on methane emissions on the seasonal and interannual time scales, Global Biogeochem. Cy., 24, GB2003, doi:10.1029/2008GB003354, 2010. 13246

BGD
9, 13243–13286, 2012

Rosenberry, D., Glaser, P., Siegel, D., and Weeks, E.: Use of hydraulic head to estimate volumetric gas content and ebullition flux in northern peatlands, Water Resour. Res., 39, 1066, doi:10.1029/2002WR001377, 2003. 13250, 13251

Roulet, N.: Peatlands, carbon storage, greenhouse gases, and the Kyoto Protocol: prospects and significance for Canada, Wetlands, 20, 605–615, doi:10.1672/0277-5212(2000)020[0605:PCSGGA]2.0.CO;2, 2000. 13246

Saarnio, S., Alm, J., Silvola, J., Lohila, A., Nykanen, H., and Martikainen, P.: Seasonal variation in CH_4 emissions and production and oxidation potentials at microsites on an oligotrophic pine fen, Oecologia, 110, 414–422, doi:10.1007/s004420050176, 1997. 13251

Severinghaus, J., Sowers, T., Brook, E., Alley, R., and Bender, M.: Timing of abrupt climate change at the end of the Younger Dryas interval from thermally fractionated gases in polar ice, Nature, 391, 141–146, doi:10.1038/34346, 1998. 13245

Shannon, R. and White, J.: 3-year study of controls on methane emissions from 2 Michigan peatlands, Biogeochemistry, 27, 35–60, 1994. 13252

Shannon, R., White, J., Lawson, J., and Gilmour, B.: Methane efflux from emergent vegetation in peatlands, J. Ecol., 84, 239–246, doi:10.2307/2261359, 1996. 13250

Singarayer, J. S., Valdes, P. J., Friedlingstein, P., Nelson, S., and Beerling, D. J.: Late Holocene methane rise caused by orbitally controlled increase in tropical sources, Nature, 470, 82–U91, doi:10.1038/nature09739, 2011. 13247

Sitch, S., Smith, B., Prentice, I. C., Arneth, A., Bondeau, A., Cramer, W., Kaplan, J. O., Levis, S., Lucht, W., Sykes, M. T., Thonicke, K., and Venevsky, S.: Evaluation of ecosystem dynamics, plant geography and terrestrial carbon cycling in the LPJ dynamic global vegetation model, Global Change Biol., 9, 161–185, 2003. 13248, 13249

Sowers, T.: Atmospheric methane isotope records covering the Holocene period, Quat. Sci. Rev., 29, 213–221, doi:10.1016/j.quascirev.2009.05.023, 2010. 13264

Spahni, R., Schwander, J., Fluckiger, J., Stauffer, B., Chappellaz, J., and Raynaud, D.: The attenuation of fast atmospheric CH_4 variations recorded in polar ice cores, Geophys. Res. Lett., 30, 1571, doi:10.1029/2003GL017093, 2003. 13245, 13246

Spahni, R., Chappellaz, J., Stocker, T., Loulergue, L., Hausammann, G., Kawamura, K., Fluckiger, J., Schwander, J., Raynaud, D., Masson-Delmotte, V., and Jouzel, J.: Atmospheric methane and nitrous oxide of the late Pleistocene from Antarctic ice cores, Science, 310, 1317–1321, doi:10.1126/science.1120132, 2005. 13247

BGD
9, 13243–13286, 2012

Spahni, R., Wania, R., Neef, L., van Weele, M., Pison, I., Bousquet, P., Frankenberg, C., Foster, P. N., Joos, F., Prentice, I. C., and van Velthoven, P.: Constraining global methane emissions and uptake by ecosystems, Biogeosciences, 8, 1643–1665, doi:10.5194/bg-8-1643-2011, 2011. 13247, 13256, 13257, 13262, 13263

Stevenson, D., Dentener, F., Schultz, M., Ellingsen, K., van Noije, T., Wild, O., Zeng, G., Amann, M., Atherton, C., Bell, N., Bergmann, D., Bey, I., Butler, T., Cofala, J., Collins, W., Derwent, R., Doherty, R., Drevet, J., Eskes, H., Fiore, A., Gauss, M., Hauglustaine, D., Horowitz, L., Isaksen, I., Krol, M., Lamarque, J.-F., Lawrence, M., Montanaro, V., Muller, J.-F., Pitari, G., Prather, M., Pyle, J., Rast, S., Rodriguez, J., Sanderson, M., Savage, N., Shindell, D., Strahan, S., Sudo, K., and Szopa, S.: Multimodel ensemble simulations of present-day and near-future tropospheric ozone, J. Geophys. Res., 111, D08301, doi:10.1029/2005JD006338, 2006. 13258

13248

Stocker, B. D., Strassmann, K., and Joos, F.: Sensitivity of Holocene atmospheric CO_2 and the modern carbon budget to early human land use: analyses with a process-based model, Biogeosciences, 8, 69–88, doi:10.5194/bg-8-69-2011, 2011.

Strassmann, K. M., Joos, F., and Fischer, G.: Simulating effects of land use changes on carbon fluxes: past contributions to atmospheric CO_2 increases and future commitments due to losses of terrestrial sink capacity, Tellus B, 60, 583–603, doi:10.1111/j.1600-0889.2008.00340.x, 2008. 13248

Strom, L., Mastepanov, M., and Christensen, T.: Species-specific effects of vascular plants on carbon turnover and methane emissions from wetlands, Biogeochemistry, 75, 65–82, doi:10.1007/s10533-004-6124-1, 2005. 13253

Tarnocai, C., Swanson D., Kimble J., and Broll G.: Northern Circumpolar Soil Carbon Database, Digital Database, Research Branch, Agriculture and Agri-Food Canada, Ottawa, Canada, available at: http://wms1.agr.gc.ca/NortherCircumpolar/northercircumpolar.zip (last access: September 2012), 2007. 13255

Tarnocai, C., Canadell, J. G., Schuur, E. A. G., Kuhry, P., Mazhitova, G., and Zimov, S.: Soil organic carbon pools in the northern circumpolar permafrost region, Global Biogeochem. Cy., 23, GB2023, doi:10.1029/2008GB003327, 2009. 13254, 13255, 13282

Tokida, T., Miyazaki, T., and Mizoguchi, M.: Ebullition of methane from peat with falling atmospheric pressure, Geophys. Res. Lett., 32, L13823, doi:10.1029/2005GL022949, 2005. 13250, 13251

BGD

9, 13243–13286, 2012

Tokida, T., Miyazaki, T., Mizoguchi, M., Nagata, O., Takakai, F., Kagemoto, A., and Hatano, R.: Falling atmospheric pressure as a trigger for methane ebullition from peatland, Global Biochem.Cy., 21, GB2003, doi:10.1029/2006GB002790, 2007. 13250, 13265

Valdes, P., Beerling, D., and Johnson, C.: The ice age methane budget, Geophys. Res. Lett., 32, L02704, doi:10.1029/2004GL021004, 2005. 13247

van Huissteden, J.: Methane emission from northern wetlands in Europe during Oxygen Isotope Stage 3, Quat. Sci. Rev., 23, 1989–2005, doi:10.1016/j.quascirev.2004.02.015, 2004. 13247

Vellinga, M. and Wood, R.: Global climatic impacts of a collapse of the Atlantic thermohaline circulation, Climatic Change, 54, 251–267, doi:10.1023/A:1016168827653, 2002. 13245

Walter, B. P., Heimann, M., and Matthews, E.: Modeling modern methane emissions from natural wetlands I. model description and results, J. Geophys. Res., 106, 34189–34206, 2001. 13246

Wania, R.: Modelling northern peatland land surface processes, vegetation dynamics and methane emissions, Ph. D. thesis, University of Bristol, 25 pp., available at: http://www.wania.net/work (not published) (last access date: September 2012), 2007. 13253, 13254

Wania, R., Ross, I., and Prentice, I. C.: Integrating peatlands and permafrost into a dynamic global vegetation model: 1. Evaluation and sensitivity of physical land surface processes, Global Biogeochem. Cy., 23, GB3014, doi:10.1029/2008GB003412, 2009a. 13247, 13248, 13249

Wania, R., Ross, I., and Prentice, I. C.: Integrating peatlands and permafrost into a dynamic global vegetation model: 2. Evaluation and sensitivity of vegetation and carbon cycle processes, Global Biogeochem. Cy., 23, GB3015, doi:10.1029/2008GB003413, 2009b. 13247, 13248, 13249

Wania, R., Ross, I., and Prentice, I. C.: Implementation and evaluation of a new methane model within a dynamic global vegetation model: LPJ-WHyMe v1.3.1, Geosci. Model Dev., 3, 565–584, doi:10.5194/gmd-3-565-2010, 2010. 13246, 13247, 13248, 13249, 13250, 13251, 13253, 13255, 13260, 13261, 13280

Weber, S. L., Drury, A. J., Toonen, W. H. J., and van Weele, M.: Wetland methane emissions during the Last Glacial Maximum estimated from PMIP2 simulations: climate, vegetation, and geographic controls, J. Geophys. Res.-Atmos., 115, D06111, doi:10.1029/2009JD012110, 2010. 13247, 13263

Weiss, R.: Solubility of nitrogen, oxygen and argon in water and seawater, Deep-sea Res., 17, 721–735, doi:10.1016/0011-7471(70)90037-9, 1970. 13251

BGD

9, 13243–13286, 2012

Wiesenburg, D. and Guinasso, N.: Equilibrium solubilities of methane, carbon-monoxide and hydrogen in water and sea-water, J. Chem. Eng. Data, 24, 356–360, doi:10.1021/je60083a006, 1979. 13251

Yamamoto, S., Alcauskas, J., and Crozier, T.: Solubility of methane in distilled water and sea-water, J. Chem. Eng. Data, 21, 78–80, doi:10.1021/je60068a029, 1976. 13251

Zhuang, Q., Melillo, J., Kicklighter, D., Prinn, R., McGuire, A., Steudler, P., Felzer, B., and Hu, S.: Methane fluxes between terrestrial ecosystems and the atmosphere at northern high latitudes during the past century: a retrospective analysis with a process-based biogeochemistry model, Global Biogeochem. Cy., 18, GB3010, doi:10.1029/2004GB002239, 2004. 13263

Zobler, L.: A World Soil File for Global Climate Modelling, NASA Technical Memorandum 87802, 1986. 13254

BGD

9, 13243–13286, 2012

Table 1. Average methane emissions before perturbation (EBP) and after perturbation (EAP) from northern peatland; standard parameters: $f_{CH_4/CO_2} = 0.17\,g\,C\,(g\,C)^{-1}$, $f_{oxid} = 0.5$, tiller radius $r_{tiller} = 0.0035\,m$, V_{gas} (fraction of gas from actual water volume) = 0.15, ΔV (fraction for ebullition) = 0.01.

Parameter	value	EBP ($Tg\,CH_4\,yr^{-1}$)	EAP ($Tg\,CH_4\,yr^{-1}$)	reduction in %
standard parameters		30.00	24.42	−18.6 %
f_{oxid}	0.2	35.48	29.48	−16.9 %
f_{oxid}	0.3	33.16	27.37	−17.5 %
f_{oxid}	0.4	31.38	25.77	−17.9 %
f_{oxid}	0.6	28.77	23.43	−18.6 %
r_{tiller}	0.00175	30.11	24.67	−18.7 %
r_{tiller}	0.007	29.56	24.12	−18.4 %
V_{gas}	0.2	29.97	24.50	−18.4 %
ΔV	0.05	30.02	24.60	−18.5 %

BGD
9, 13243–13286, 2012

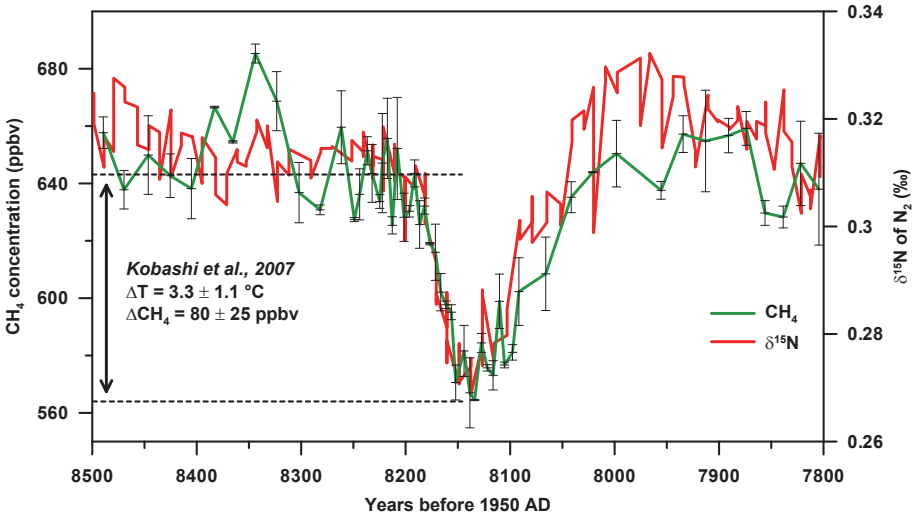

Fig. 1. Evolution of Greenland temperature and atmospheric methane concentration during the 8.2 kyr event. The measured δ^{15}N signature allows for a quantitative temperature reconstruction and represents a temperature change of about 3 °C over Central Greenland which is accompanied by an 80 ppbv decline in atmospheric CH_4 (Kobashi et al., 2007).

BGD
9, 13243–13286, 2012

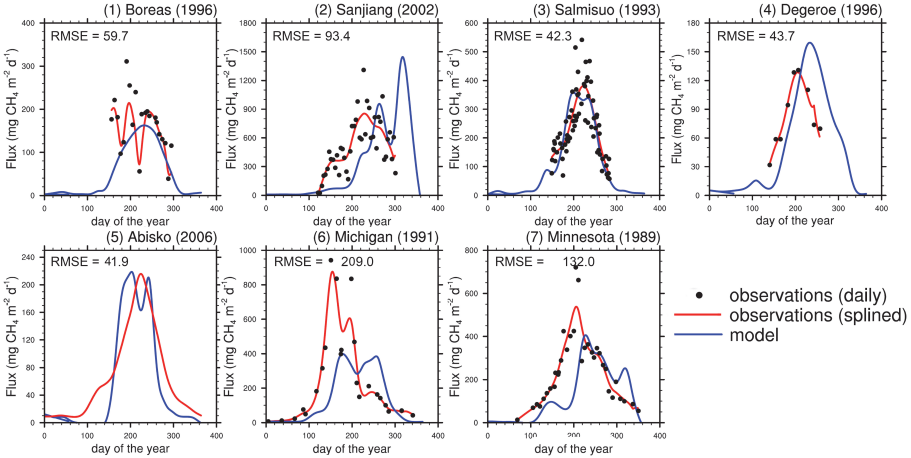

Fig. 2. Daily methane emissions measured at seven sites compared to LPJ model output analogue to a previous model calibration (Wania et al., 2010). All our model runs use the same optimised parameter set for all sites. The respective root mean square errors (RMSE) are given in the top left corner of each box. Note that at the Degeroe site ebullition was not measured and was therefore also excluded in the model output. The Abisko record is the only one with daily measurements. Model results are plotted as smoothing spline function with a cut-off period of two months (blue line), observations are plotted as daily values (black dots) and a smoothing spline function with a cut-off period of two months (red line). Note the different scales on the y-axes.

BGD
9, 13243–13286, 2012

Impact of an 8.2-kyr-like event on methane emissions in northern peatlands

S. Zürcher et al.

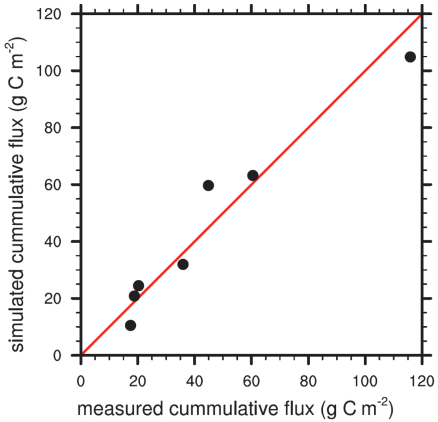

Fig. 3. Measured versus simulated cumulative methane emissions for each site. Emissions for each site are integrated over the time spanned by the measurements.

BGD
9, 13243–13286, 2012

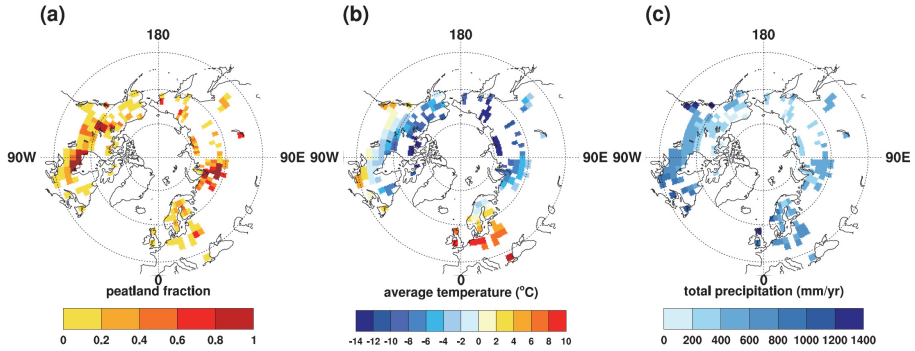

Fig. 4. Distribution and grid cell fraction of peatlands based on (Tarnocai et al., 2009) for present conditions **(a)**; Northern Hemisphere climate patterns averaged over 1961–1990 CRU data (New et al., 1999; Mitchell and Jones, 2005) for temperature **(b)** and precipitation **(c)**, at the peatland grid cells.

BGD
9, 13243–13286, 2012

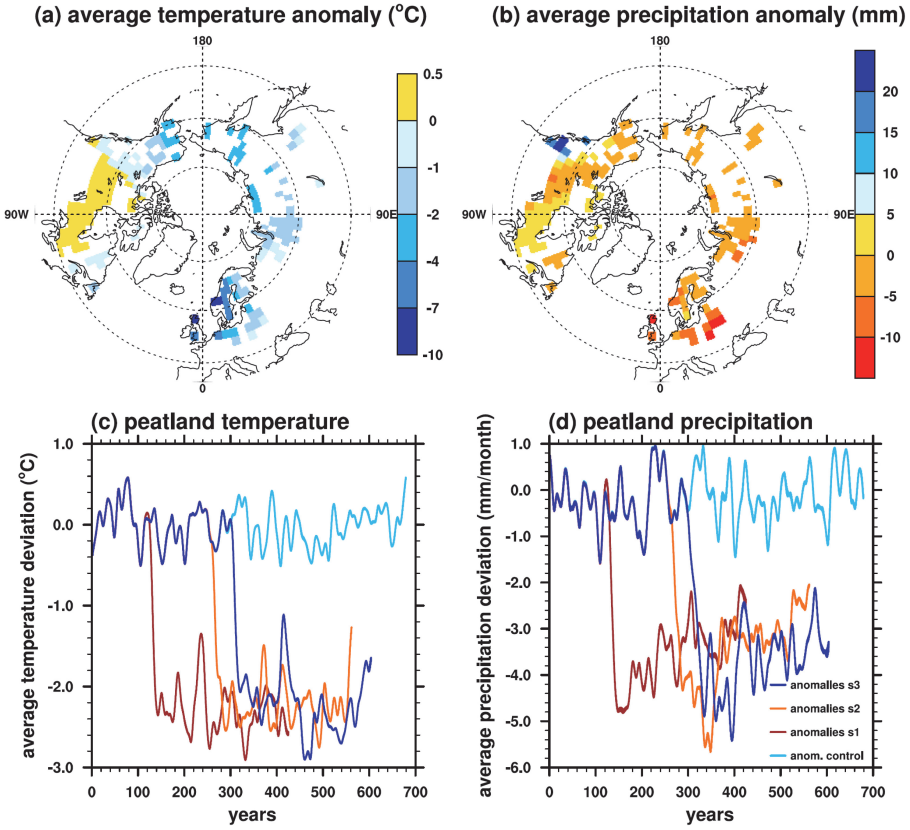

Fig. 5. Temperature and precipitation anomalies in boreal peatlands simulated by NCAR CSM 1.4 in response to freshwater hosing in the North Atlantic. Top: anomalies represent the differences in 50 yr averages of monthly data before and after the freshwater release of ensemble run 1. Bottom: anomalies represent spatial-averages using peatland area of each grid cell as weights and with respect to the mean of the control simulation (2 months running average).

BGD
9, 13243–13286, 2012

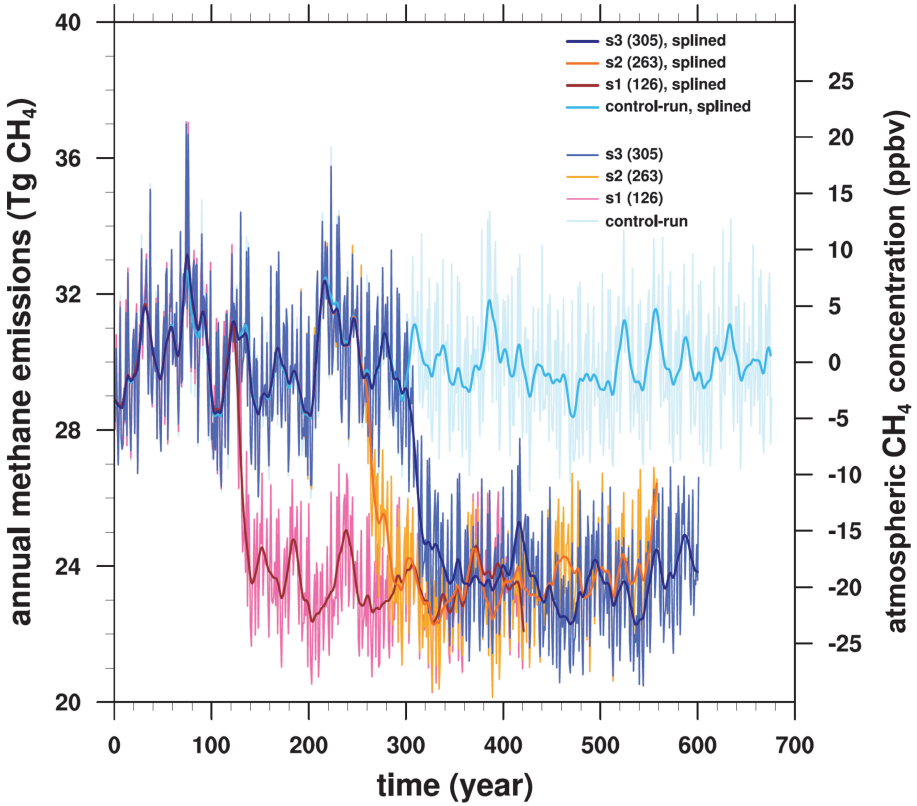

Fig. 6. Total methane emission from northern peatlands for the ensemble runs with freshwater input forcing (s1 to s3) and the control run (cyan). The resulting total methane flux was scaled to reach an average value of 30 Tg CH_4 per year during the control run. Annual emissions are shown by light colors and splines through the annual data by dark colors.

BGD
9, 13243–13286, 2012

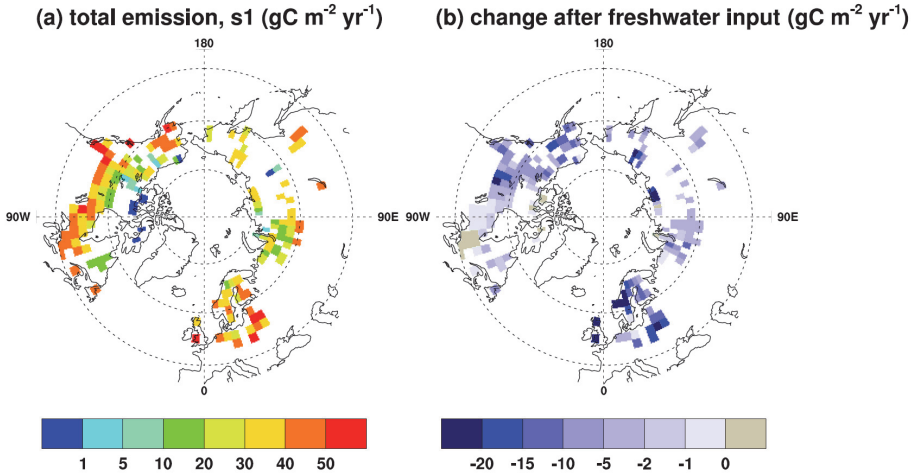

Fig. 7. (a) Spatial distribution of methane emissions ($gC\,m^{-2}yr^{-1}$) from the sum of plant-mediated transport, diffusion and ebullition averaged over the first fifty years of the control run. **(b)** Difference in methane emission ($gC\,m^{-2}yr^{-1}$) in 50-yr averages of monthly data before and after the freshwater release of ensemble run 1.

BGD
9, 13243–13286, 2012

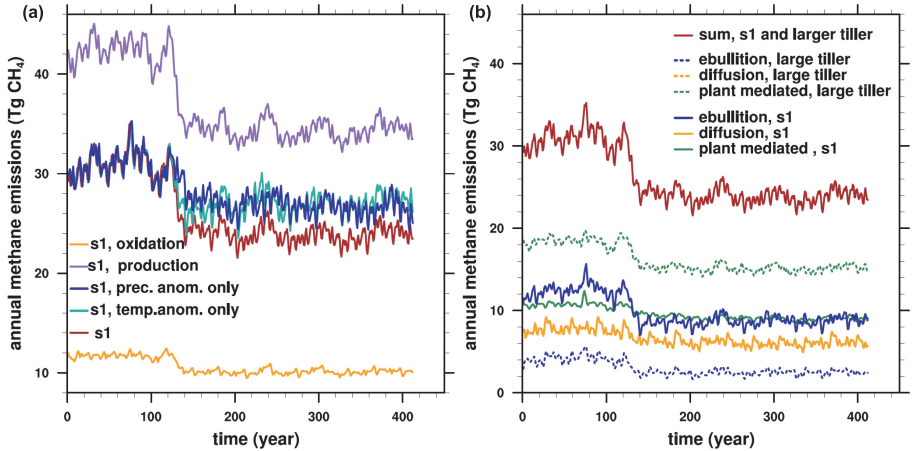

Fig. 8. (a) Total annual methane emission from northern peatlands (red) compared to factorial runs where only changes in temperature (cyan) or only in precipitation (blue) were taken in account. The total annual methane production rate (violet) and soil oxidation rate (yellow) is plotted as well. **(b)** Contribution of the three different transport pathways to the total emissions. Results are obtained with the best fitting parameters (solid lines) and a run with a doubled tiller-radius (dashed lines). The total emissions and emissions by diffusion are identical, whereas there is a redistribution of plant-mediated emissions and emissions by ebullition. Climate forcing data are from ensemble simulation s1 and model output is smoothed with a spline.

BGD
9, 13243–13286, 2012